Optics Communications 338 (2015) 95–100

Contents lists available at ScienceDirect

Optics Communications

journal homepage: www.elsevier.com/locate/optcom

Polarization imaging with enhanced spatial resolution

A. Peinado [a,*], A. Lizana [a], C. Iemmi [b], J. Campos [a]

[a] Departament de Física, Universitat Autònoma de Barcelona, 08193 Bellaterra, Spain
[b] Departamento de Física, FCEN, Universidad de Buenos Aires, 1428 Buenos Aires, Argentina

ARTICLE INFO

Article history:
Received 1 July 2014
Received in revised form
8 September 2014
Accepted 14 September 2014
Available online 29 October 2014

Keywords:
Superresolution
Polarimetry
Spatial light modulators
Liquid-crystal devices
Stokes vector

ABSTRACT

We present the design and the experimental implementation of a new imaging set-up, based on Liquid Crystal technology, able to obtain super-resolved polarimetric images of polarimetric samples when the resolution is detector limited. The proposed set-up is a combination of two modules. One of them is an imaging Stokes polarimeter, based on Ferroelectric Liquid Crystal cells, which is used to analyze the polarization spatial distribution of an incident beam. The other module is used to obtain high resolved intensity images of the sample in an optical system whose resolution is mainly limited by the CCD pixel geometry. It contains a calibrated Parallel Aligned Liquid Crystal on Silicon display employed to introduce controlled linear phases. As a result, a set of different low resolved intensity images with sub-pixel displacements are captured by the CCD. By properly combining these images and after applying a deconvolution process, a super-resolved intensity image of the object is obtained. Finally, the combination of the two different optical modules permits to employ super-resolved images during the polarimetric data reduction calculation, leading to a final polarization image with enhanced spatial resolution. The proposed optical set-up performance is implemented and experimentally validated by providing super-resolved images of an amplitude resolution test and a birefringent resolution test. A significant improvement in the spatial resolution (by a factor of 1.4) of the obtained polarimetric images, in comparison with the images obtained with the regular imaging system, is clearly observed when applying our proposed technique.

1. Introduction

Spatial resolution (SR) is a measure for the ability to distinguish two separated points in an image. SR is limited by diverse factors: numerical aperture of the imaging system, the wavelength of the employed light, misalignments and aberrations of the optical components, geometrical properties of the camera pixel (size, shape and pitch) among others [1]. High resolution devices are required for many purposes in imaging based applications, such as in remote sensing applications [2] or for medical purposes [3]. Different approaches have been reported to attempt to overcome the resolution of an imaging system. As well known, one of the main limitations for the SR is the diffraction limit of the optical system. To overcome this limitation different super-resolution methods have been presented in the literature, as for instance those based on the use of diffraction gratings [4], structured illumination [5,6] and time multiplexing super-resolution techniques [7]. In the case of modern imaging systems, they usually include Charged-Coupled Device (CCD) cameras as the main devices to capture the images. In such cases, the pixel dimension of the camera may also impose a geometrical limitation in resolution. In particular, many optical systems have detector pixels relatively large compared to the point spread function (PSF) of the optical system, resulting in a system that is undersampled. In such systems, the optical system passes higher spatial frequencies than those that the detector can correctly sense. Undersampled systems are used in some applications because they may present some interesting advantages, such as improved sensitivity leading to faster integration times and higher signal-to-noise ratio (SNR), larger fields-of-view, better image quality and less expensive [8,9]. When the SR is limited by the detector pixels, geometry multiframe super-resolution algorithms can be employed to improve the resolution of the imagery, as for instance sight-and-add, interlacing, Drizzle algorithm, [10] techniques based on the maximum likelihood [11,12], projection onto convex sets [13,14], non uniform interpolations [15,16], stochastic reconstruction method [17,18], code-division multiplexing [19], among others [9,20,21].

In general, imaging systems only analyze the intensity information of an object. However, extra image information, as an accurate knowledge of the light polarization content, may be of interest in some applications. For instance, in medical applications [22,23], polarimetric images provide valuable data for diagnosis, being this information hidden in regular intensity images of the

* Corresponding author.
E-mail address: alba.peinado@uab.es (A. Peinado).

http://dx.doi.org/10.1016/j.optcom.2014.09.079
0030-4018/

sample. Imaging polarimeters are the basic devices to perform these polarization images, as those described in [24,25].

Moreover, the analysis of the polarimetric information collected in high numerical aperture imaging systems may help to resolve details of the object beyond the resolution limit. For instance, in [26] the position and orientation of nanostructures are resolved beyond the diffraction limit using the spatial distribution of the azimuth angle and the degree of polarization. Another example is provided in [27], where an instrument measuring scattering-angle-resolved Mueller matrix is described allowing for a high sensitivity to sub-resolution displacements of a sub-resolution scatterer.

In this work, we propose a new imaging system, based on Liquid Crystal (LC) technology, able to obtain polarization images with enhanced spatial resolution, when the main limitation in resolution is imposed by the pixel pitch of the Charged-Coupled Device (CCD) camera. As following detailed, the experimental set-up combines a super-resolution module (which reconstructs a single high resolution image of a scene from a set of regular images recorded at lower resolution) with an imaging Stokes polarimeter (which determines the polarization spatial distribution of a light beam from a set of super-resolved intensity images obtained with the super-resolution module).

2. Experimental set-up: combination of an imaging stokes polarimeter and an intensity super-resolution module

The proposed set-up sketched in Fig. 1 is implemented in the laboratory. A collimated red light emitting diode (LED, $\lambda_o = 625$ nm and $\Delta\lambda = 17$ nm) is used to illuminate the system. Then, a Polarizing State Generator (PSG), consisting of a linear polarizer (LP_1) and a quarter waveplate (QWP), is used to manipulate the polarization of the incident beam illuminating the scene. After the scene, the Stokes polarimeter is placed, working as a Polarization State Analyzer (PSA). This system is composed by two monopixel ferroelectric liquid crystal (FLC) cells and a second linear polarizer (LP_2). A convergent lens (L) images the scene onto the CCD plane, obtaining low resolved images due to the pixel size limitation of the CCD. Nevertheless, we include an extra module for enhancing the spatial resolution of the intensity images taken by the camera. In this module the light is transmitted by a 50/50 non polarizing beam splitter (B-S) towards a Parallel Aligned Liquid Crystal on Silicon (PA-LCoS) display. This device is a pure phase spatial light modulator (SLM) that allows the introduction of linear phases very precisely controlled. The reflected light goes back to the B-S and is redirected to the detector. The linear phases generate sub-pixel displacements of the low-resolution images at the CCD plane, and by combining them and applying an anti-aliasing algorithm it is possible to reconstruct a final super resolved intensity image. Finally, by combining 4 super-resolved intensity images, and conducting a polarimetric data reduction calculation later explained, a super-resolved polarimetric image is obtained.

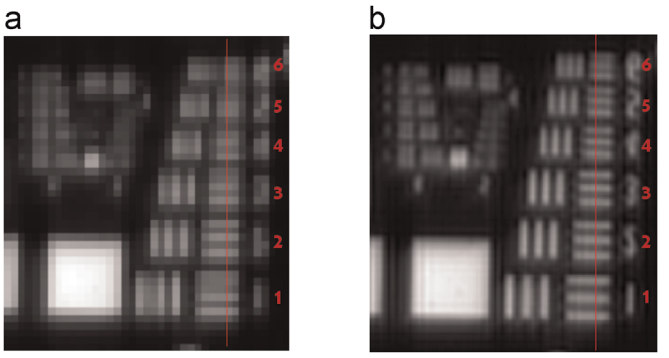

Fig. 2. S_0 Stokes element of USAF resolution test by applying (a) the regular technique and (b) the enhanced resolution technique. Cross sections of the red lines are plotted in Fig. 3. (For interpretation of the references to color in this figure legend, the reader is referred to the web version of this article.)

The PA-LCoS display used in this work is a PLUTO SLM distributed by HoloEye Systems with a diagonal display of 1.8 cm, a resolution of 1920×1080 pixels, with a pixel pitch of 8 μm and a fill factor of 87%. To operate with the PA-LCoS in the phase-only regime, the LP_2 is orientated at the same direction than the LC molecules extraordinary axis.

The ideal experimental set-up should use a transmissive liquid crystal display (LCD), avoiding the use of the B-S and its corresponding light losses. However, the available LCD in our laboratory is a PA-LCoS display working in reflection. So, a set-up configuration working in reflection is required. Under this scenario, two possible configurations could be used: a B-S based set-up or an off-axis illumination based set-up. However, the LCD phase modulation range decreases as the incidence angle increases [28], for this reason we have selected the layout of Fig. 1.

We are looking for the increase of resolution at the image plane, where the pixel size and point spread function (PSF) size are of concern. For the optical imaging system configuration employed, the PSF is about a quarter of the pixel size. Thus, the spatial

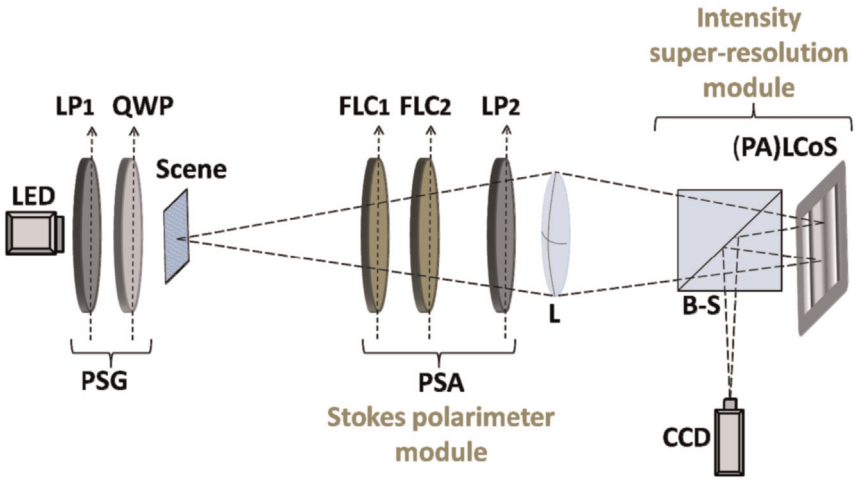

Fig. 1. Experimental set-up used to implement the polarization imaging system with enhanced spatial resolution. This consists of two parts: an imaging Stokes polarimeter (two Ferroelectric Liquid Crystal cells and a polarizer) and an intensity super-resolution module (LCoS spatial light modulator).

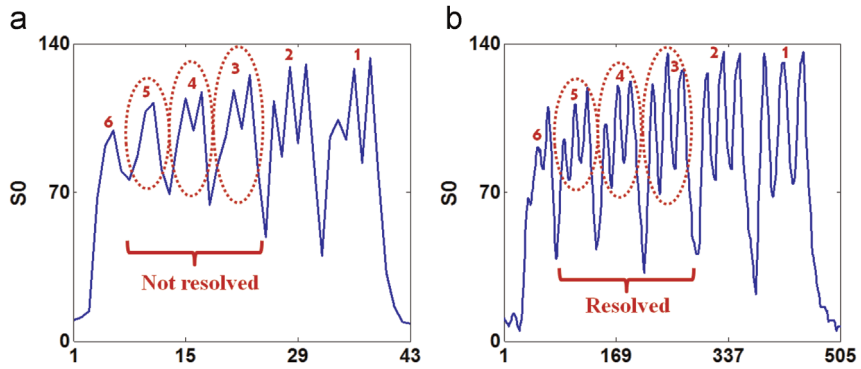

Fig. 3. Cross section of the S_0 element of the USAF test as function of the y pixel position (red line in Fig. 2). Experimental data when applying: (a) the regular technique and (b) the enhanced resolution technique.

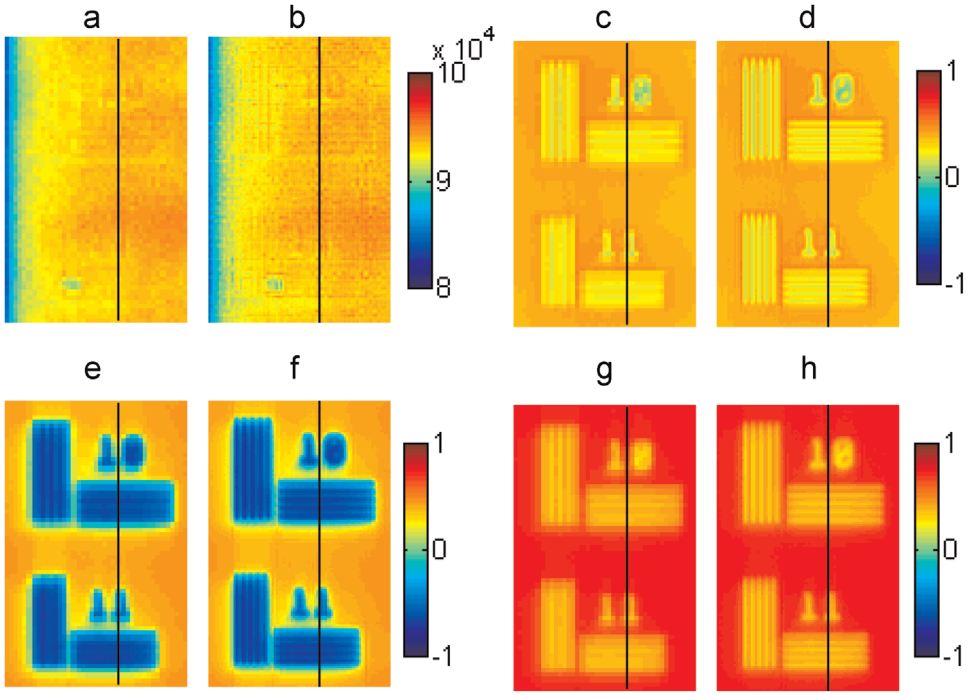

Fig. 4. Polarization image of a birefringent resolution test obtained by applying the two techniques. Regular resolution Stokes parameters: (a) S_0, (c) S_1, (e) S_2 and (g) S_3. Enhanced resolution Stokes parameters: (b) S_0, (d) S_1, (f) S_2 and (h) S_3. Cross sections of the black lines are plotted in Fig. 5.

resolution of our imaging system is limited by the pixel size of the camera.

2.1. Intensity super-resolution module

To achieve super-resolved intensity images of a scene by using the super-resolution module included in Fig. 1, we apply the imaging super-resolution algorithm described in [29]. This algorithm is suitable to increase the Spatial Resolution (SR) of the final scene image when the SR is mainly limited by the CCD pixels dimension. Basically, a linear phase is introduced by the PA-LCoS to shift the image over the CCD plane a sub-pixel distance. To this end, the SLM phase-to-voltage response must be accurately calibrated, as well as the relationship between the linear phase displayed at the PA-LCoS and the corresponding image displacement produced at the CCD plane. Once the sub-pixel displacements are controlled, a set of $n_x \cdot n_y$ sub-pixel 2-D displacements are generated with the SLM, where n_x and n_y are the number of displacements in x and y directions, respectively. In this situation, $n_x \cdot n_y$ images are recorded. The dimension of each raw image is (s_x,s_y). Afterwards, raw images are interlaced in a larger image of dimension $(n_x \cdot s_x,\ n_y \cdot s_y)$. Note that all raw images suffer the intensity spatial average due to the pixel size, causing blurring effect [20,29]. Thus, the final image of larger dimension, created by properly interlacing those raw images, will be consequently affected by the same blurring effect. From a mathematical point of view, the intensity detected by the camera can be described as the convolution of the scene intensity distribution ($I(x,y)$) with the shape of the camera pixel ($p(x,y)$):

$$I_d(x, y) = I(x, y) \otimes p(x, y). \tag{1}$$

In order to remove this blurring effect, an inverse filtering process is applied in the frequency domain [30,31]. The goal of the algorithm is to isolate the intensity distribution ($I(x,y)$), eliminating as much as possible the effect of the pixel size ($p(x,y)$). To this aim, we first multiply the Fourier transform (FT) of the intensity detected by the camera ($\tilde{I}_d$) with the filter (f), as shown in [29, 31]:

$$\tilde{I}_{filtered}(u, \nu) = \tilde{I}_d(u, \nu) \cdot f(u, \nu) = \frac{\tilde{I}_d(u, \nu)\tilde{p}^*(u, \nu)}{|\tilde{p}(u, \nu)|^2 + \sigma}, \tag{2}$$

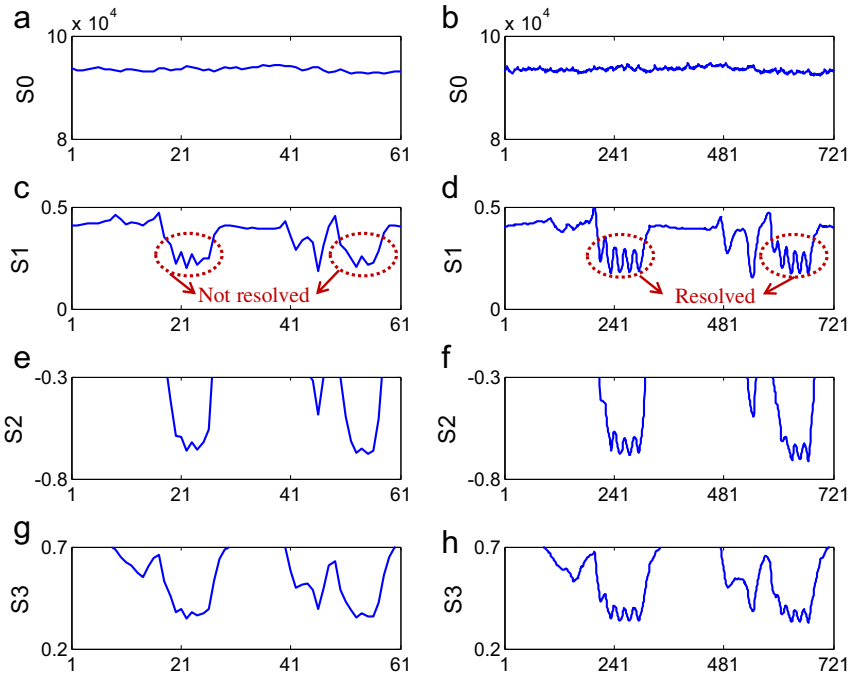

Fig. 5. Cross section of the birefringent resolution test measurements shown in Fig. 4. Regular resolution Stokes parameters: (a) S_0, (c) S_1, (e) S_2 and (g) S_3. Enhanced resolution Stokes parameters: (b) S_0, (d) S_1, (f) S_2 and (h) S_3. All Stokes elements are given as function of the y pixel position.

where $\tilde{I}_{filtered}(u, v)$ is the Fourier transform of the synthesized intensity image of the object, $\tilde{p}^*(u, v)$ and $|\tilde{p}(u, v)|$ are the complex conjugate and absolute value of the *FT* of the pixel shape respectively and, σ is a parameter which takes small values and is used to avoid possible zeros at the denominator of Eq. (2). In fact, $f(u,v)$ is the so-called Wiener filter [31], where we have considered that the images are mainly affected by white noise and the constant σ is related with its spectral density. When the spectral density is not known, it is necessary to select a proper value of this constant. If it is too small, the noise will be much amplified, on the contrary when it is too big, the blurring effect is not removed.

Finally, we perform the inverse Fourier transform of $\tilde{I}_{filtered}(u, v)$, obtaining the synthesized intensity image of the object. By applying this technique we are able to obtain super-resolved images of the object due to the blurring effect has been removed to certain extent.

2.2. Imaging Stokes polarimeter

The Stokes polarimeter integrated in our set-up is described in detail in [32] and here summarized. We used a polarimeter based on liquid crystal panels in order to avoid experimental errors typically associated to polarimeters based on rotating elements [33], as beam wander or misalignments. Moreover, FLC cells have a very fast response, allowing us to implement a polarimeter with high measurement rate (in our case, in the order of milliseconds). A FLC can be modeled as a linear retarder of fix retardance and two stable orientations for its fast axis, switchable when addressing a square electrical signal [34]. The FLC cells used in our set-up have a nominal retardance of $\lambda/2$ and $\lambda/4$ (FLC_1 and FLC_2 respectively in Fig. 1). Then, by synchronously addressing two square signals of period T and $T/2$ to the FLC panels, four different combinations of the FLCs orientations are obtained during a period T and so, four different polarization analyzers are implemented in the PSA. The measurement principle of a Stokes polarimeter is defined by the following expression:

$$I = WS, \tag{3}$$

where S is the Stokes vector of the incident light (i.e. our unknown), W is the polarimetric measurement matrix, containing information of the four polarization analyzers used to characterize the incident beam, and I is a vector with a set of intensity measurements. Each intensity measurement is the result of projecting the incident beam over a particular polarization analyzer. Once the matrix W is calibrated, it can be inverted as it is formed by a set of four independent polarization analyzers. Hence, the Stokes vector is completely determined as:

$$S = W^{-1}I, \tag{4}$$

where W^{-1} is the inverse matrix of W, and it is called the polarimetric data reduction matrix. Note that noise in the intensity measurements will be amplified through the matrix W^{-1} to the Stokes vector. In order to minimize the noise propagation during data reduction, an optimization of the orientations of the FLC cells is conducted [32]. In particular, the condition number criterion [35] is followed. This parameter indicates how close the matrix W is to a unitary matrix, which does not amplify error. The best optimized polarimeter would have a CN of 1.73, and it leads to a noise equalization in the Stokes channels [36]. However, the optimized FLC based polarimeter configuration has a CN of 2.22, leading to small differences between the Stokes channels noise response. Particularly, the variances associated to the Stokes parameters S_0, S_1, S_2 and S_3 are, respectively, 1.0, 3.1, 4.9 and 2.1.

The punctual Stokes polarimeter described in [32] is extended in this work to an image Stokes polarimeter (see Fig. 1). In this way, it is possible to calculate the Stokes vector distribution by means of 4 intensity images, where Eq. (4) is applied individually for each pixel of the CCD camera. Therefore, an image where each pixel contains information about the azimuth, ellipticity and degree of polarization of the beam at that particular position is obtained.

Note that one of the main novelties present in our method lies on not using regular intensity images for the data reduction process but using the high resolved intensity images provided by the super-resolved module present in Fig. 1. In this way, we apply super-resolved intensity images of the scene for the polarimetric

data reduction calculation and consequently, we are able to achieve a final polarimetric image with enhanced resolution. As above mentioned, to provide super-resolved images of the scene, we are using the super-resolution method described in Section 2.1. This method is very useful when the main resolution limitation in the system is related to the pixel dimensions of the CCD camera. However, we want to emphasize the potential of including an LCoS display in the proposed set-up. In particular, different super-resolution techniques based on LCoS technology are proposed in the literature [6,37], which are not addressed to detector-limited resolution but to diffraction-limited resolution. Therefore, by conducting some modifications in the super-resolution module in the experimental set-up, the concept of using super-resolved images for polarimetry analysis could be adapted and tested for other origins of the optical system resolution limit.

3. Experimental results

Particularly, in our work the enhanced SR technique is achieved by producing sub-pixel displacements of 1/12 the pixel size in both x and y directions. We want to note that the timing imaging and processing in our experimental set-up depends on different factors, as the transitory time of the FLC panels, the number of n subpixels selected, the exposure time of the camera, the number of images to be averaged and the processing time of the computer, among others. For the experimental results provided in this work, none of these parameters have been optimized in terms of time minimization. On the contrary, we have set some security times to ensure a proper synchronization between the FLC panels and the camera, and ultimately a suitable performance for the super-resolution imaging polarimeter. Therefore, the complete measuring and processing time leading to the super-resolved polarimetric images is roughly about 5 min. However, if this time needs to be reduced for requirements of a particular application, the number of subpixel displacements as well as the others parameters stated above could be optimized.

Some preliminary steps are conducted before testing the SR enhancement in polarimetric images. First, we have used the eigenvalue calibration method (ECM) [38] to calibrate the Stokes polarimeter. Once the polarimetric measurement matrix W is known, our polarimeter is validated by studying its capability of measuring different incident States of Polarization (SoPs). In particular, different beams with spatially uniform polarization are generated with the PSG system, and later, measured with the Stokes polarimeter, obtaining a standard deviation smaller than 10^{-3}. Afterwards, the polarimetric system with the intensity super-resolution module is validated by measuring two different spatial resolution tests: the first one has non uniform spatial transmission and uniform polarimetric properties and the second one has uniform transmission but non uniform spatial polarimetric properties.

First, in order to test the spatial resolution enhancement achieved in the intensity content by applying the described technique, a 1951-USAF resolution target (Newport, model RES-1) was used as amplitude scene. The object consists on several arrangements of 3 horizontal and 3 verticals lines, labeled with a number that sorts them by the spatial frequency of each particular arrangement. The Stokes vector element S_0 (i.e. the total intensity of the beam) obtained with regular imaging is represented in Fig. 2(a)), whereas the counterpart obtained with the enhanced resolution algorithm is shown in Fig. 2(b). We observe a clear improvement in the spatial resolution in both directions. Focusing on the right side of the images, it is noticeable that the different groups of frequencies not resolved in Fig. 2(a) are better resolved in Fig. 2(b). In order to quantitatively demonstrate this improvement, the cross sections of the red lines marked in Fig. 2 are represented in Fig. 3. Comparing both plots present in Fig. 3, we observe that groups labeled with the number 3, 4 and 5 (circled with dashed lines) when applying the enhanced SR technique (Fig. 3(b)) are resolved, whereas when applying the regular imaging (Fig. 3(a)) are not resolved. In particular, the enhanced SR technique reaches to the element 5 (12.70 cycles/mm), whereas the regular technique only reaches to the element 2 (8.98 cycles/mm), leading to an improvement of resolution by a factor of 1.4. Consequently, we assert that the algorithm improves the spatial resolution in intensity images.

Second, with the aim of testing the resolution enhancement in polarimetric images, a birefringence resolution target (Thorlabs model NBS 1963A) is used as a scene. It consists on a birefringent pattern sandwiched between two glass substrates. The pattern includes different groups of birefringent material with different spatial frequencies but with uniform transmission. Each group, sorted in two sets of five horizontal lines and five vertical lines, is labeled with a number referring to the cycles per mm.

The Stokes vectors of the input object were measured when the scene was illuminated with linearly polarized light. Fig. 4 shows the Stokes vector elements obtained from regular polarization measurement (Fig. 4(a,c,e,g)) and from the enhanced SR measurement (Fig. 4(b,d,f,h)). As expected, the object has uniform S_0, due to the uniform transmission of the pattern. Moreover, it is noticeable that the different frequency groups are only distinguishable through the S_1, S_2 and S_3 elements, because of the non-uniform polarimetric spatial distribution.

To differentiate polarimetric data from intensity images, as those depicted in Fig. 2, and to emphasize that the resolution improvement is achieved in polarimetric images, we have used a pseudocolor mapping to show the Stokes elements S_0, S_1, S_2 and S_3. In general, it is observed that the images obtained with the proposed technique offers much better resolution than the ones obtained from regular measurements. In order to show in more detail the resolution enhancement in the polarimetric images, the vertical cross sections corresponding to the black lines marked in Fig. 4, are plotted in Fig. 5. Note that cross sections of S_1–S_3 Stokes parameters in Fig. 5 are zoomed in the Y axis including a range of 0.5 (the full Stokes scale goes from -1 up to 1). This is done to better visualize how the different frequency arrangements of interest are resolved by the experimental system.

It is observed that Stokes elements S_1, S_2 and S_3 (Fig. 5(d,f,h), respectively) are much better resolved when applying the super resolution technique than the ones using the regular technique (Fig. 5(c,e,g), respectively). As an example, the dashed circles plotted in Fig. 5 point out that whereas the 5 consecutive lines per group are clearly resolved when applying the enhancing SR algorithm (Fig. 5(d)), they cannot be resolved by applying a regular method (Fig. 5(c)). Note that Figs. 4 and 5 represent a region of interest of the whole birefringent resolution target. This sample area is selected to highlight the resolution improvement that we have observed between both techniques. When the polarimetric images corresponding to the entire resolution test are analyzed, we observe that the largest resolved frequency in the best case (S_1 channel) reaches 9 cycles/mm for regular imaging, whereas super-resolving imaging reaches 12.5 cycles/mm, leading to an improvement of resolution by a factor of 1.4. Certainly, the polarization measurement with enhanced resolution technique resolves intermediate states of polarization between two birefringent lines, whereas in regular images those zones are not resolved.

Note that S_1 and S_3 channels present better resolution than S_2 channel. This fact may be due to the inhomogenous noise response of the Stokes polarimeter, in agreement with the Stokes variances values shown above (Stokes variance S_2 is larger than S_1 and S_3). Moreover, polarimetric data are given in multichannel images,

thus the contrast of these images depend on the channel analyzed, as it can be observed in Fig. 5. Particularly, S_1 has larger contrast than S_2 and S_3 channels. This contrast not only depends on the original object, but also could depend on the coordinate system chosen to define the state of polarization. In addition, it will depend on the state of polarization of the beam illuminating the scene, which could be also optimized as function of the scene to be measured [39]. This study is an interesting perspective to this work, although is beyond the scope of this paper.

4. Conclusions

Summarizing, we have presented a new experimental set-up able to obtain super-resolved polarimetric images, when the spatial resolution of the system is limited by the pixel size of the imaging device. The proposed and implemented experimental set-up consists of two parts: an imaging Stokes polarimeter and an intensity super-resolution module.

On one hand, the intensity super-resolution module is based on a Parallel Aligned Liquid Crystal on Silicon display where different linear phases are addressed. After calibrating the response of the spatial modulator, it is possible to generate sub-pixel displacements of the image at the CCD plane. By combining these low resolved images and after applying a deconvolution process, a final super-resolved image of larger dimension than the original ones is obtained. The technique leads to a significantly improvement in the spatial resolution of an image when this is limited by the pixel geometry of the CCD camera. On the other hand, an imaging Stokes polarimeter based on Ferroelectric Liquid Crystal cells is used in the experimental set-up to analyze the polarization spatial distribution of the incident beam.

Our novel approach consists of using the super-resolved intensity images in the polarimetric data reduction calculation, obtaining as a result, polarimetric images with enhanced spatial resolution. Different spatial resolution test targets (in amplitude and in birefringence) have been measured. The experimental results show a significant improvement in spatial resolution by a factor of 1.4 for intensity and polarimetric images, when the proposed technique is applied.

Finally, we remark that by taking profit of the polyvalence of the SLM device, the super-resolution module could be modified to apply other super-resolution imaging techniques [6,37]. In this way, when the main resolution limitation on the imaging system is not originated by the CCD pixel size, a more suitable super-resolution technique, based on SLM technology, should be selected.

Acknowledgments

We acknowledge financial support from the Spanish MINECO (FIS2012-39158-C02-01, and fondos FEDER) and the Catalan Government (SGR2009-00347). C. Iemmi thanks the support of UBACyT 20020100100689, CONICET PIP 112-200801-03047, and ANPCYT PICT 2010-02179 (Argentina).

References

[1] Z. Zalevsky, D. Mendlovic, Optical Superresolution, Springer, New York, 2003.
[2] A. Tatem, Super-resolution land cover pattern prediction using a Hopfield neural network, Remote Sens. Environ. 79 (2002) 1–14.
[3] H. Greenspan, Super-resolution in medical imaging, Comput. J. 52 (2008) 43–63.
[4] W. Lukosz, Optical systems with resolving powers exceeding the classical limit II, J. Opt. Soc. Am. 57 (1967) 932–939.
[5] V. Mico, Z. Zalevsky, P. Garcia-Martinez, J. Garcia, Single-step superresolution by interferometric imaging, Opt. Express 12 (2004) 2589.
[6] A. Hussain, J.L. Martínez, A. Lizana, J. Campos, Super resolution imaging achieved by using on-axis interferometry based on a Spatial Light Modulator, Opt. Express 21 (2013) 9615–9623.
[7] A. Calabuig, V. Micó, J. Garcia, Z. Zalevsky, C. Ferreira, Single-exposure super-resolved interferometric microscopy by red-green-blue multiplexing, Opt. Lett. 36 (2011) 885–887.
[8] R.D. Fiete, Image quality and λFN/p for remote sensing systems, Opt. Eng. 38 (7) (1999) 1229–1240.
[9] S.C. Park, M.K. Park, M.G. Kang, Super-resolution image reconstruction: a technical overview, IEEE Signal Process. Mag. 20 (3) (2003) 21–36.
[10] A.S. Fruchter, R.N. Hook, A novel image reconstruction method applied to deep Hubble space telescope images, Proc. SPIE 3164 (1997) 120–125.
[11] M.S. Alam, J.G. Bognar, S. Cain, B.J. Yasuda, Fast registration and reconstruction of aliased low-resolution frames by use of a modified maximum-likelihood approach, Appl. Opt. 37 (1998) 1319–1328.
[12] S. Farsiu, M.D. Robinson, M. Elad, P. Milanfar, Fast and robust multiframe super resolution, IEEE Trans. Image Process 13 (2004) 1327–1344.
[13] H. Stark, P. Oskoui, High-resolution image recovery from image-plane arrays, using convex projections, J. Opt. Soc. Am. A 6 (1989) 1715–1726.
[14] A.M. Tekalp, M.K. Ozkan, and M.I. Sezan, High-resolution image reconstruction from lower-resolution image sequences and space varying image restoration, in: Proceedings of IEEE International Conference on Acoustics, Speech and Signal Processing (ICASSP) 3 (1992) pp. 169–172.
[15] H. Ur, D. Gross, Improved resolution from sub-pixel shifted pictures, CVGIP, Gr. Models Image Process. 54 (1992) 181–186.
[16] T. Komatsu, K. Aizawa, T. Igarashi, T. Saito, Signal-processing based method for acquiring very high resolution image with multiple cameras and its theoretical analysis, Proc. Inst. Electr. Eng. 140 (1) (1993) 19–25.
[17] P. Cheeseman, B. Kanefsky, R. Kraft, J. Stutz, R. Hanson, Super-resolved surface reconstruction from multiple images, in Maximum Entropy and Bayesian Methods, Springer Netherlands, Santa Barbara (1996) 293–308.
[18] R.C. Hardie, K.J. Barnard, E.E. Armstrong, Joint MAP registration and high-resolution image estimation using a sequence of undersampled images, IEEE Trans. Image Process. 6 (1997) 1621–1633.
[19] J. Solomon, Z. Zalevsky, D. Mendlovic, Geometric superresolution by code division multiplexing, Appl. Opt. 44 (2005) 32.
[20] A. Shemer, D. Mendlovic, Z. Zalevsky, J. Garcia, P. Garcia Martinez, Super-resolving optical system with time multiplexing and computer decoding, Appl. Opt. 38 (1999) 7245.
[21] A. Borkowski, Z. Zalevsky, B. Javidi, Geometrical superresolved imaging using nonperiodic spatial masking, J. Opt. Soc. Am. A 26 (2009) 589.
[22] A. Pierangelo, S. Manhas, A. Benali, C. Fallet, J.-L. Totobenazara, M.-R. Antonelli, et al., Multispectral Mueller polarimetric imaging detecting residual cancer and cancer regression after neoadjuvant treatment for colorectal carcinomas, J. Biomed. Opt. 18 (2013) 046014.
[23] K.M. Twietmeyer, R.A. Chipman, A.E. Elsner, Y. Zhao, D. VanNasdale, Mueller matrix retinal imager with optimized polarization conditions, Opt. Express 16 (2008) 21339.
[24] N.J. Pust, J.A. Shaw, Dual-field imaging polarimeter using liquid crystal variable retarders, Appl. Opt. 45 (2006) 5470.
[25] L. Gendre, A. Foulonneau, L. Bigué, Imaging linear polarimetry using a single ferroelectric liquid crystal modulator, Appl. Opt. 49 (2010) 4687.
[26] O.G. Rodríguez-Herrera, D. Lara, C. Dainty, Far-field polarization-based sensitivity to sub-resolution displacements of a sub-resolution scatterer in tightly focused fields, Opt. Express 18 (2010) 5609–5628.
[27] C. Macias-Romero, M.R. Foreman, P.R.T. Munro, P. Török, Confocal polarization imaging in high-numerical-aperture space, Opt. Lett. 39 (2014) 2322.
[28] A. Lizana, N. Martín, M. Estapé, E. Fernández, I. Moreno, A. Márquez, C. Iemmi, J. Campos, M.J. Yzuel, Influence of the incident angle in the performance of liquid crystal on silicon displays, Opt. Express 17 (10) (2009) 8491–8505.
[29] M. Sohail, A. Lizana, J. Campos, Super-resolution imaging technique based on a liquid crystal on silicon display: increase of charge-coupled device resolution limit, Ópt. Pura Y Apl. 46 (2013) 223–230.
[30] J.C. Russ, The Image Processing Handbook, CRC Press, Boca Raton, 2011.
[31] R.C. González, R.E. Woods, Digital Image Processing, Pearson Prentice Hall, New Jersey, 2008.
[32] A. Peinado, A. Lizana, J. Campos, Optimization and tolerance analysis of a polarimeter with ferroelectric liquid crystals, Appl. Opt. 52 (2013) 5748–5757.
[33] D.H. Goldstein, R.A. Chipman, Error analysis of a Mueller matrix polarimeter, J. Opt. Soc. Am. A 7 (1990) 693.
[34] A. Martínez, N. Beaudoin, I. Moreno, M.D.M. Sánchez-López, P. Velásquez, Optimization of the contrast ratio of a ferroelectric liquid crystal optical modulator, J. Opt. A Pure Appl. Opt. 8 (2006) 1013–1018.
[35] P. Taylor, Theory and Applications of Numerical Analysis, second ed., Academic Press, London, 1996.
[36] J.S. Tyo, Noise equalization in Stokes parameter images obtained by use of variable-retardance polarimeters, Opt. Lett. 25 (16) (2000) 1198–1200.
[37] A. Hussain, J.L. Martinez, J. Campos, Holographic superresolution using spatial light modulator, J. Eur. Opt. Soc. Rapid Publ. 8 (2013) 13007.
[38] E. Compain, S. Poirier, B. Drevillon, General and self-consistent method for the calibration of polarization modulators, polarimeters, and Mueller-matrix ellipsometers, Appl. Opt. 38 (1999) 3490–3502.
[39] F. Goudail, Optimization of the contrast in active Stokes images, Opt. Lett. 34 (2009) 121–123.